

Sparse Layered MIMO with Iterative Detection

Mohamad H. Dinan, Nemanja Stefan Perović, *Member, IEEE*, and Mark F. Flanagan, *Senior Member, IEEE*

Abstract—In this paper, we propose a novel transmission scheme, called *sparse layered MIMO* (SL-MIMO), that combines non-orthogonal transmission and singular value decomposition (SVD) precoding. Non-orthogonality in SL-MIMO allows re-using of the eigen-channels which improves the spectral efficiency and error rate performance of the system through enhancing the coding gain and diversity gain. We also present a low-complexity message-passing (MP) detector for the proposed SL-MIMO system which performs quite close to maximum likelihood (ML). The joint moment generating function (MGF) of the ordered eigenvalues is calculated and used to derive a closed-form upper bound on the average word error probability (AWEP) of the SL-MIMO system, and this derived expression is then used to analyze the diversity gain of the system. We use our analytical results to design sub-optimal codebooks to minimize the error rate of the SL-MIMO system. Simulation results in 4×4 and 6×6 multiple-input multiple-output (MIMO) systems with 4-ary, 16-ary, and 64-ary constellations show that our proposed SL-MIMO scheme outperforms competing approaches such as X- and Y-codes in terms of system error rate performance. SL-MIMO has 5.6 dB advantage compared to X-codes and 4.7 dB advantage compared to Y-codes in 6×6 MIMO system with a 64-ary constellation.

Index Terms—Multiple-input multiple-output (MIMO), precoding, code-domain non-orthogonal transmission, spatial coding, joint moment generating function (MGF) of ordered eigenvalues.

I. INTRODUCTION

Multiple-input multiple-output (MIMO) systems represent a key technology in wireless communications, as they can substantially improve both the reliability and the data rate [1]. For a MIMO system with channel state information available at the transmitter, the precoding technique based on singular value decomposition (SVD) of the channel matrix is optimal with respect to the capacity and error rate performance measures [2]. The reason for this is that standard SVD precoding decomposes the MIMO channel into multiple parallel independent eigen-channels [1], [3], and an appropriate power allocation across the eigen-channels can optimize different performance criteria [4]–[7]. Hence, maximum likelihood (ML) detection at the receiver can be performed independently for each eigen-channel. The downside of the standard SVD precoding, where the power allocation is realized by a diagonal matrix, is that the diversity gain is determined by the smallest eigenvalue; therefore, there is a trade-off between the diversity gain and data rate. However, it was shown in [8] that a non-diagonal precoding matrix can improve the performance of the MIMO

system in terms of the average bit error rate (BER). Another non-diagonal precoding approach was proposed in [9] for a system with only two eigen-channels, based on maximizing the minimum distance of the received symbols. Motivated by [9], non-diagonal MIMO precoding schemes based on pairing good and bad eigen-channels have been proposed in [10]–[12] for larger MIMO systems to improve the BER performance through increasing the diversity gain of the system. In [10], the authors proposed a non-diagonal cross-form matrix as an online precoder¹ with the aim of maximizing the minimum Euclidean distance within pairs of eigen-channels. The so-called X- and Y-codes/precoders were proposed in [11]. X-codes/precoders use rotated constellations within a pair of eigen-channels in order to minimize the average word error probability (AWEP), while Y-codes/precoders were designed to maximize the minimum Euclidean distance by performing rate and power allocation within a pair of eigen-channels. Another cross-form precoder design was proposed in [12] to improve the error rate performance while allowing low-complexity decoding. Despite the efficient design of these precoders, all of the aforementioned *pairing* approaches suffer from interference within each pair of eigen-channels, specifically at higher data rates. Besides, they need to be adapted to each channel realization to perform more efficiently, since all of these precoders, other than Y-codes, do not consider the stochastic properties of the eigenvalues of the channel matrix.

On the other hand, code-domain non-orthogonal transmission has been considered as a promising technology within modern wireless communications to improve the spectral efficiency by sharing (re-using) the same resource elements (REs) [13]–[16]. Low density signature (LDS) [17], [18] and sparse code multiple access (SCMA) [19] are two prominent examples of this approach. In LDS, each user sparsely spreads its data over the available REs. Therefore, the interference pattern can be represented by a low-density factor graph, and a corresponding low-complexity message-passing (MP) detector can be implemented at the receiver. The basic structure of SCMA is similar to that of LDS, however, in SCMA, instead of spreading a symbol, each user transmits different symbols over its available REs. The potential of SCMA has motivated researchers to investigate the application of non-orthogonal transmission to MIMO systems. In this regard, various *MIMO-SCMA* system designs have been developed [20]–[27]. In [20], the authors analyzed the performance of a multi-layer spatial multiplexing (SMX) MIMO system combined with SCMA. The performance of MIMO-SCMA systems designed based on vertical Bell Labs layered space-time (VBLAST) and

This work was funded by the Irish Research Council (IRC) under the Consolidator Laureate Award Programme (grant number IRCLA/2017/209).

Mohamad H. Dinan, Nemanja Stefan Perović, and Mark F. Flanagan are with School of Electrical and Electronic Engineering, University College Dublin, Belfield, Dublin 4, Ireland (Email: mohamad.hejazidinan@ucdconnect.ie, nemanja.stefan.perovic@ucd.ie, mark.flanagan@ieec.org).

¹The terms “precoder” and “code” are defined in [11] to distinguish between “online” and “offline” design of the precoding matrices. A *precoder* is dedicated to each channel realization and needs to be adaptively changed, while a *code* can be designed offline *a priori*.

space-time block code (STBC) was investigated in [21]. The concept of spatial modulation (SM) has also been considered in MIMO-SCMA systems in [22]–[25] and the corresponding error rate performance of these systems has been analyzed. The authors in [26] proposed a multi-dimensional STBC (MSTBC) MIMO-SCMA system to exploit the transmit diversity. In [27], the concept of generalized spatial modulation (GSM) was used in a MIMO-SCMA system utilizing STBC in order to provide a framework for uplink transmission to increase the transmit diversity and reduce the hardware complexity of mobile users. In addition, various detection techniques have been proposed to reduce the complexity and improve the performance of the MIMO-SCMA system [28]–[31]. However, in all of the aforementioned studies, code-domain non-orthogonal transmission have been applied to either the *time* or *frequency* domain, similar to the case of single-input single-output (SISO)-SCMA, and the concept of non-orthogonal transmission in the *spatial domain* has not yet been applied to design MIMO precoding. In addition to the above-mentioned advantages of precoding, sharing and re-using the eigen-channels can further enhance the spectral efficiency and error rate performance of a MIMO system.

Against this background, in this paper we introduce a new paradigm for MIMO precoding based on applying code-domain non-orthogonal transmission across eigen-channels. In particular, the structure of the code is designed to carefully control the interference among eigen-channels. The contributions of this paper are as follows:

- Inspired by code-domain non-orthogonal transmission, we propose a novel MIMO scheme which uses SVD precoding along with a sparse non-diagonal matrix to allow re-use of the eigen-channels, which we call *sparse layered MIMO* (SL-MIMO). We exploit SVD precoding to create a set of eigen-channels which we use as orthogonal REs. Then, we split the input data bits into layers and spread the corresponding symbols over the eigen-channels in a sparse manner.
- We propose a sub-optimal MP detection algorithm for SL-MIMO, which has a significantly lower decoding complexity than ML detection. We show that the MP detector performance exhibits fast convergence and has a performance very close to that of ML.
- We analyze the AWEP of the SL-MIMO system, and derive a closed-form upper bound on the AWEP which is tight at high signal-to-noise ratio (SNR). This requires evaluation of the joint moment generating function (MGF) of the *ordered* eigenvalues, which to the best of the authors' knowledge has not been previously provided in the literature. Moreover, we perform an asymptotic analysis of the AWEP of the proposed system and determine its diversity gain.
- A sub-optimal approach is proposed for designing the sparse codebooks for the layers, in order to minimize the AWEP of the system. We formulate a joint optimization problem to determine the multidimensional constellations for all layers. We then define a multi-step sub-optimal approach to simplify the procedure. In each step, we aim

to minimize the asymptotic AWEP for a set of layers. The multi-step design procedure has a low complexity and only needs to be performed once offline. In this way, the SL-MIMO approach is categorized as a “code” and not as a “precoder” [11], i.e., the constellations are designed *a priori* and do not change with each channel realization.

- Finally, we investigate the performance of the system through numerical simulations. The results show substantial improvement over competing approaches such as X- and Y-codes, especially at higher data rates. The superiority increases at higher data rates and in larger MIMO systems.

The rest of this paper is organized as follows. We describe the SL-MIMO system model in Section II. In Section III, the analysis of the AWEP, including its asymptotic analysis, is presented. Section IV describes the constellation design procedure for the SL-MIMO system. Numerical results and comparisons with other relevant schemes are provided in Section V. Finally, Section VI concludes this paper.

Notation: Boldface lower-case letters indicate column vectors, and boldface upper-case letters indicate matrices. \mathbf{I}_n represents an $n \times n$ identity matrix, and $\mathbf{0}_{n \times m}$ indicates an $n \times m$ zero matrix. The superscripts $(\cdot)^T$ and $(\cdot)^H$ denote transpose and Hermitian transpose, respectively. $\text{diag}(\cdot)$ converts a vector into a corresponding diagonal matrix. $\|\cdot\|$ denotes the Euclidean norm of a vector, and $|\cdot|$ denotes the cardinality of a set. The set $\{1, 2, \dots, K\}$ is represented by $[K]$. $\mathbb{E}\{\cdot\}$ denotes the expectation operator. Finally, the set of complex numbers is denoted by \mathbb{C} .

II. SYSTEM MODEL

Fig. 1 shows a block diagram of the proposed SL-MIMO system. We consider a point to point communication system, whose transmitter and receiver employ N_t and N_r antennas, respectively. The elements of the channel matrix $\mathbf{H} \in \mathbb{C}^{N_r \times N_t}$ are i.i.d complex Gaussian random variables with zero mean and unit variance. The received signal is given by

$$\mathbf{y} = \mathbf{H}\mathbf{x} + \mathbf{n}, \quad (1)$$

where $\mathbf{x} \in \mathbb{C}^{N_t \times 1}$ is the *transmit vector*, and $\mathbf{n} \in \mathbb{C}^{N_r \times 1}$ is the noise vector which is distributed according to $\mathcal{CN}(0, N_0 \mathbf{I}_{N_r})$. We use the SVD precoding technique to decompose the channel into a set of parallel virtual channels (or eigen-channels). The SVD of the channel matrix \mathbf{H} can be expressed as $\mathbf{H} = \mathbf{U}\mathbf{\Sigma}\mathbf{V}^H$, where $\mathbf{U} \in \mathbb{C}^{N_r \times N_r}$ and $\mathbf{V} \in \mathbb{C}^{N_t \times N_t}$ are unitary matrices, and $\mathbf{\Sigma} = \begin{bmatrix} \mathbf{\Lambda}^{\frac{1}{2}}, \mathbf{0}_{N_r \times (N_t - N_r)} \end{bmatrix}$ for $N_r < N_t$, or $\mathbf{\Sigma} = \begin{bmatrix} \mathbf{\Lambda}^{\frac{1}{2}}, \mathbf{0}_{N_t \times (N_r - N_t)} \end{bmatrix}^T$ for $N_r \geq N_t$, where $\mathbf{\Lambda} = \text{diag}(\boldsymbol{\lambda} = [\lambda_1, \dots, \lambda_n]^T)$ and $\{\lambda_m\}$ are the eigenvalues of the matrix $\mathbf{H}\mathbf{H}^H$ ($N_r < N_t$) or $\mathbf{H}^H\mathbf{H}$ ($N_r \geq N_t$), such that $n = \min(N_t, N_r)$ and $\lambda_1 \geq \lambda_2 \geq \dots \geq \lambda_n \geq 0$. SVD transmission implies that at the transmitter, the *data symbol vector* $\mathbf{s} = [s_1, \dots, s_n]^T$ is mapped to the transmit vector \mathbf{x} via $\mathbf{x} = \mathbf{V}\mathbf{s}$, while at the receiver, the received vector \mathbf{y} is pre-multiplied by the matrix \mathbf{U}^H , where \mathbf{V} and \mathbf{U} are sub-matrices

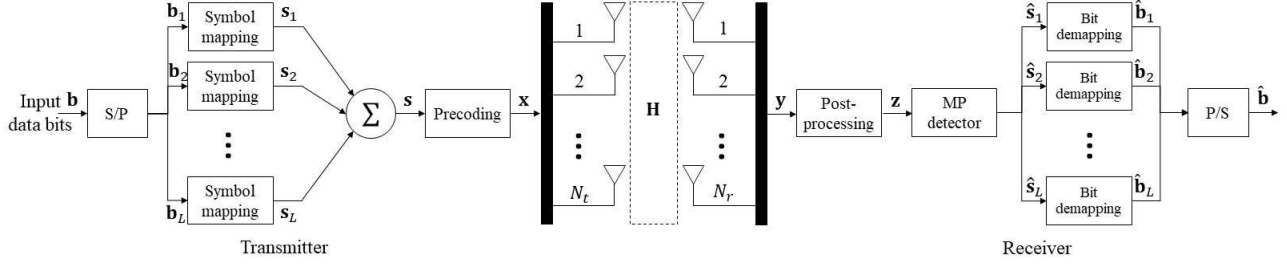


Fig. 1. Transmitter and receiver structure for the proposed sparse layered MIMO (SL-MIMO) system.

consisting of the first n columns of \mathbf{V} and \mathbf{U} , respectively. Then, the post-processed received signal vector is given as

$$\mathbf{z} \triangleq \bar{\mathbf{U}}^H \mathbf{y} = \mathbf{\Lambda}^{\frac{1}{2}} \mathbf{s} + \mathbf{n}', \quad (2)$$

where $\mathbf{n}' \in \mathbb{C}^{n \times 1}$ is the post-processed noise vector which has the same distribution as \mathbf{n} . The system in (2) consists of n parallel eigen-channels with channel gains $\{\sqrt{\lambda_m}\}$, which are used as orthogonal resources to transmit sparse coded symbols.

In the proposed SL-MIMO system, each block of $\eta = L \times \log_2 M$ bits in the data bit stream \mathbf{b} is split into L equal-sized packets \mathbf{b}_l ; each $\log_2 M$ -bit packet \mathbf{b}_l represents the data bits for layer l , and is encoded into a sparse codeword $\mathbf{s}_l = [s_{l,1}, \dots, s_{l,n}]^T$ of length n . The codeword \mathbf{s}_l is selected from a pre-designed codebook \mathcal{S}_l for layer l , having size M (for the sake of simplicity, we assume that the codebooks of all layers are equal in size). Thus, the system achieves a spectral efficiency of η bits per channel use (bpcu).

Each codebook \mathcal{S}_l is *sparse*, in the sense that only n_l of the n entries of any codeword consist of nonzero in-phase and quadrature (IQ) symbols; the remainder of the entries are equal to zero. The set of nonzero positions for codebook \mathcal{S}_l is denoted by $\mathcal{N}_l \subset \{1, 2, \dots, n\}$, and so we have $|\mathcal{N}_l| = n_l$. Thus, for $m \in \mathcal{N}_l$, entry $s_{l,m}$ in \mathbf{s}_l is then the IQ symbol for layer l which is transmitted over eigen-channel m . The number of layers that share the m -th eigen-channel is denoted by d_m , and $\mathcal{D}_m \subset \{1, 2, \dots, L\}$ is the set of the interfering layers at eigen-channel m . The connectivity between the eigen-channels and the layers can be represented by a binary sparse layering (SL) matrix (similar to the parity-check matrix of a low-density parity-check (LDPC) code) whose rows corresponds to eigen-channels and columns corresponds to layers; its (m, l) -entry $a_{m,l}$ is equal to 1 if and only if layer l uses eigen-channel m .

As an example, we consider the SL matrix

$$\mathbf{A} = \begin{bmatrix} 1 & 1 & 1 & 0 & 0 & 0 \\ 1 & 0 & 0 & 1 & 1 & 0 \\ 0 & 1 & 0 & 1 & 0 & 1 \\ 0 & 0 & 1 & 0 & 1 & 1 \end{bmatrix} \quad (3)$$

which corresponds to the case where $n = 4$ and $L = 6$. It can be deduced from the first column of this matrix that layer 1 uses eigen-channels 1 and 2, i.e., $\mathcal{N}_1 = \{1, 2\}$, and that eigen-channel 1 is used by layers 1, 2 and 3, i.e., $\mathcal{D}_1 = \{1, 2, 3\}$. We also note that the matrix \mathbf{A} in (3) is a *regular* matrix, which means that the number of ones in rows and in columns are

fixed for all eigen-channels and layers, respectively. In other words $n_l = 2$ for all l , and $d_m = 3$ for all m .

The length- n data symbol vector is then formed by adding the codewords for each layer, i.e.,

$$\mathbf{s} = \sum_{l=1}^L \mathbf{s}_l, \quad (4)$$

so that we have

$$s_m = \sum_{l \in \mathcal{D}_m} s_{l,m}, \quad \forall m, \quad (5)$$

Then, we define \mathcal{S} to be set of all possible data symbol vectors \mathbf{s} . In addition, we impose the following design condition on the codebooks $\{\mathcal{S}_l\}$: we assume that the codebooks satisfy the property that any two vectors in \mathcal{S} differ in some position m only if there exists at least one layer sharing eigen-channel m in which the chosen codewords also differ, i.e., for any vectors $\mathbf{s}^{(1)} = \sum_{l=1}^L \mathbf{s}_l^{(1)}$ and $\mathbf{s}^{(2)} = \sum_{l=1}^L \mathbf{s}_l^{(2)}$, it holds that for every $m \in \{1, 2, \dots, n\}$

$$\mathbf{s}_m^{(1)} \neq \mathbf{s}_m^{(2)} \quad \text{only if} \quad \mathbf{s}_l^{(1)} \neq \mathbf{s}_l^{(2)} \quad \text{for at least one } l \in \mathcal{D}_m. \quad (6)$$

Also, for ease of exposition, we assume that all codebooks have the same average energy E_s , i.e.,

$$\mathbb{E} \left\{ \|\mathbf{s}_l\|^2 \right\} = E_s, \quad l = 1, \dots, L. \quad (7)$$

Finally, we assume that input data bits of different layers are independent, so that the total transmit power of the system is

$$P_t = \mathbb{E} \left\{ \|\mathbf{x}\|^2 \right\} = \mathbb{E} \left\{ \|\mathbf{s}\|^2 \right\} = \mathbb{E} \left\{ \left\| \sum_{l=1}^L \mathbf{s}_l \right\|^2 \right\} = LE_s,$$

where the second equality holds since $\bar{\mathbf{V}}^H \bar{\mathbf{V}} = \mathbf{I}_n$, and the final equality holds due to the aforementioned independence assumption. Hence, the SNR is equal to P_t/N_0 .

With these properties, the SL-MIMO system can be considered as a generalized SVD precoding system, with additional degrees of freedom. Also, it is worthwhile to note that the X- and Y-codes of [11] may be viewed as special cases of SL-MIMO. The corresponding SL matrices of X- and Y-codes have the shape of the letters X and Y, respectively. For

example, the SL matrices of X- and Y-codes for a system with 4 eigen-channels are respectively given by

$$\mathbf{A}_X = \begin{bmatrix} 1 & 0 & 0 & 1 \\ 0 & 1 & 1 & 0 \\ 0 & 1 & 1 & 0 \\ 1 & 0 & 0 & 1 \end{bmatrix}, \mathbf{A}_Y = \begin{bmatrix} 1 & 0 & 0 & 1 \\ 0 & 1 & 1 & 0 \\ 0 & 1 & 0 & 0 \\ 1 & 0 & 0 & 0 \end{bmatrix}.$$

The structure of X- and Y-codes essentially minimizes overlap between eigen-channels, and allows for separate (independent) detection on each pair of eigen-channels. On the other hand, we allow for a controlled (and carefully designed) overlap between eigen-channels, which results in an *interference diversity* that can improve the performance, while we use MP detection in order to keep the receiver complexity low.

A. Optimal (Maximum Likelihood) Detection

At the receiver, the optimum maximum likelihood (ML) detector is given by

$$\hat{\mathbf{s}} = \arg \min_{\mathbf{s} \in \mathcal{S}} \left\{ \left\| \mathbf{z} - \mathbf{\Lambda}^{\frac{1}{2}} \mathbf{s} \right\|^2 \right\}. \quad (8)$$

Recalling (4), we have $|\mathcal{S}| = \prod_{l=1}^L |\mathcal{S}_l| = M^L$; thus the complexity of ML detection is $\mathcal{O}(M^L)$.

B. Message-Passing Algorithm

ML detection of SL-MIMO is too complex for practical implementation, especially for large values of M and L . Hence, in the following we propose the use of a message-passing (MP) algorithm for detection in the SL-MIMO system, in which the receiver exploits the sparsity of the underlying factor graph to detect the received symbols with a lower complexity (the ML detector will later be used as a benchmark to validate the MP detection results).

The decisions $\{\hat{\mathbf{s}}_1, \hat{\mathbf{s}}_2, \dots, \hat{\mathbf{s}}_L\}$ are obtained by marginalizing the function $P(\mathbf{s}_1, \mathbf{s}_2, \dots, \mathbf{s}_L | \mathbf{z})$, which is proportional to

$$p(\mathbf{z} | \mathbf{s}_1, \mathbf{s}_2, \dots, \mathbf{s}_L) P(S) = \prod_{m=1}^n P(z_m | S_m) \prod_{l=1}^L P(\mathbf{s}_l), \quad (9)$$

where S denotes the collection of all variables \mathbf{s}_l , and S_m denotes the collection of all variables \mathbf{s}_l for $l \in \mathcal{D}_m$. The factor graph then has a variable node for each variable \mathbf{s}_l , and a factor node z_m corresponding to each factor

$$P(z_m | S_m) = \frac{1}{\pi N_0} \exp \left(-\frac{1}{N_0} \left| z_m - \sqrt{\lambda_m} \sum_{l \in \mathcal{D}_m} s_{l,m} \right|^2 \right). \quad (10)$$

The MP algorithm can then be described as follows. The algorithm is initialized via

$$\mu_{\mathbf{s}_l \rightarrow z_m}^0(\mathbf{s}_l) = 1 \text{ for all } m, l \in \mathcal{D}_m, \text{ and } \mathbf{s}_l \in \mathcal{S}_l.$$

Then, MP detection proceeds as follows, where N denotes the total number of iterations. For each $t = 1$ to N , compute

$$\mu_{\mathbf{s}_l \rightarrow z_m}^t(\mathbf{s}_l) = \sum_{\{\mathbf{s}_{l'}\}, l' \in \mathcal{D}_m \setminus \{l\}} P(z_m | S_m) \prod_{l' \in \mathcal{D}_m \setminus \{l\}} \mu_{\mathbf{s}_{l'} \rightarrow z_m}^{t-1}(\mathbf{s}_{l'}) \quad (11)$$

and

$$\mu_{\mathbf{s}_l \rightarrow z_m}^t(\mathbf{s}_l) = \prod_{m' \in \mathcal{N}_l \setminus \{m\}} \mu_{z_{m'} \rightarrow \mathbf{s}_l}^t(\mathbf{s}_l) P(\mathbf{s}_l) \quad (12)$$

which, introducing a scaling factor, can be rewritten as

$$\mu_{\mathbf{s}_l \rightarrow z_m}^t(\mathbf{s}_l) = \prod_{m' \in \mathcal{N}_l \setminus \{m\}} \mu_{z_{m'} \rightarrow \mathbf{s}_l}^t(\mathbf{s}_l) \quad (13)$$

for $\mathbf{s}_l \in \mathcal{S}_l$, and $\mu_{z_m \rightarrow \mathbf{s}_l}^t(\mathbf{s}_l) = 0$ otherwise. Finally, decisions are made via

$$\hat{\mathbf{s}}_l = \arg \max_{\mathbf{s}_l \in \mathcal{S}_l} P(\mathbf{s}_l) \prod_{m \in \mathcal{N}_l} \mu_{z_m \rightarrow \mathbf{s}_l}^N(\mathbf{s}_l). \quad (14)$$

The MP detector exploits the *interference diversity* among the layers and eigen-channels. This diversity helps the MP detector to efficiently update the messages in each iteration. The complexity of the MP detector is dominated by (11), where the *a posteriori* probabilities of $\{z_m\}$ are computed, and its complexity depends on the number of interfering layers at the eigen-channels. Therefore, the overall complexity of the MP detector is $\mathcal{O}(M^{d_{\max}})$, where $d_{\max} = \max_m \{d_m\}$.

III. PERFORMANCE ANALYSIS

In this section, we analyze the average word error probability (AWEP) of the proposed SL-MIMO system. This AWEP analysis will later be used for codebook design in Section IV. Our analysis will focus on ML detection, as this is more tractable than that of the MP detector and also provides an upper bound on the achievable performance of the MP detector; moreover, as we will show later in Section V, this upper bound becomes very tight at high SNR. The AWEP can be calculated by finding the pairwise error probability (PEP) associated with data symbol vectors \mathbf{s} and $\hat{\mathbf{s}}$:

$$\begin{aligned} \text{PEP}(\mathbf{s}, \hat{\mathbf{s}}) &= \Pr(\mathbf{s} \rightarrow \hat{\mathbf{s}} | \mathbf{\Lambda}) \\ &= \Pr \left(\left\| \mathbf{z} - \mathbf{\Lambda}^{\frac{1}{2}} \mathbf{s} \right\|^2 > \left\| \mathbf{z} - \mathbf{\Lambda}^{\frac{1}{2}} \hat{\mathbf{s}} \right\|^2 \right) \\ &= \Pr \left(\left\| \mathbf{\Lambda}^{\frac{1}{2}} (\mathbf{s} - \hat{\mathbf{s}}) \right\|^2 < 2\Re \left\{ (\mathbf{s} - \hat{\mathbf{s}})^H \mathbf{\Lambda}^{\frac{1}{2}} \mathbf{n}' \right\} \right) \\ &= \mathbb{Q} \left(\sqrt{\frac{\left\| \mathbf{\Lambda}^{\frac{1}{2}} (\mathbf{s} - \hat{\mathbf{s}}) \right\|^2}{2N_0}} \right) \\ &= \mathbb{Q} \left(\sqrt{\frac{\sum_{m=1}^n \lambda_m |\psi_m|^2}{2N_0}} \right), \end{aligned} \quad (15)$$

where $\boldsymbol{\psi} = [\psi_1, \psi_2, \dots, \psi_n]^T = \mathbf{s} - \hat{\mathbf{s}}$ is the *difference vector* for this symbol vector pair. The evaluation of the average PEP requires use of the joint probability density function (PDF) of the eigenvalues. The joint PDF of the *ordered* eigenvalues $\lambda_1 \geq \lambda_2 \geq \dots \geq \lambda_{n-1} \geq \lambda_n$ is given by [32]

$$p(\boldsymbol{\lambda}) = \frac{1}{C_{N_t, N_r}} \prod_m e^{-\lambda_m} \lambda_m^{|N_t - N_r|} \prod_{m > m'} (\lambda_m - \lambda_{m'})^2, \quad (16)$$

where C_{N_t, N_r} is a normalizing factor. After expanding the polynomial, it can be written as

$$p(\boldsymbol{\lambda}) = \frac{1}{C_{N_t, N_r}} \sum_{p=1}^P \alpha_p \prod_m e^{-\lambda_m} \lambda_m^{\beta_{p,m}}, \quad (17)$$

where P indicates the number of the terms in $p(\boldsymbol{\lambda})$, and α_p and $\beta_{p,m}$ are the coefficients of the p -th monomial and the exponent of λ_m in that monomial, respectively.

Using the upper bound of Q -function [33]

$$Q(x) \leq \frac{1}{12} e^{-\frac{x^2}{2}} + \frac{1}{4} e^{-\frac{2x^2}{3}}, \quad (18)$$

the average PEP can be expressed as

$$\begin{aligned} \overline{\text{PEP}}(\mathbf{s}, \hat{\mathbf{s}}) &= \mathbb{E}_{\boldsymbol{\lambda}} \left\{ Q \left(\sqrt{\frac{\sum_m \lambda_m |\psi_m|^2}{2N_0}} \right) \right\} \\ &\leq \mathbb{E}_{\boldsymbol{\lambda}} \left\{ \frac{1}{12} \prod_m e^{-\frac{\lambda_m |\psi_m|^2}{4N_0}} + \frac{1}{4} \prod_m e^{-\frac{\lambda_m |\psi_m|^2}{3N_0}} \right\} \\ &= \frac{1}{12} M_{\boldsymbol{\lambda}}(-\mathbf{a}) + \frac{1}{4} M_{\boldsymbol{\lambda}}(-\mathbf{b}) \\ &= \frac{1}{12} \underbrace{\int \dots \int_{\mathcal{D}_{ord}} \prod_m e^{-\frac{\lambda_m |\psi_m|^2}{4N_0}} p(\boldsymbol{\lambda}) d\boldsymbol{\lambda}}_{I_1(\boldsymbol{\psi})} \\ &\quad + \frac{1}{4} \underbrace{\int \dots \int_{\mathcal{D}_{ord}} \prod_m e^{-\frac{\lambda_m |\psi_m|^2}{3N_0}} p(\boldsymbol{\lambda}) d\boldsymbol{\lambda}}_{I_2(\boldsymbol{\psi})}, \quad (19) \end{aligned}$$

where $\mathbf{a} = [a_1, a_2, \dots, a_n]^T$ and $a_m = \frac{|\psi_m|^2}{4N_0}$ for each m , $\mathbf{b} = [b_1, b_2, \dots, b_n]^T$ and $b_m = \frac{|\psi_m|^2}{3N_0}$ for each m (note that each coefficient a_m and b_m is proportional to the SNR), $M_{\boldsymbol{\lambda}}(\boldsymbol{\chi}) = \mathbb{E}_{\boldsymbol{\lambda}} \left\{ \prod_{m=1}^n e^{\chi_m \lambda_m} \right\}$ is the joint MGF of the eigenvalues, and the multiple integral is over the domain $\mathcal{D}_{ord} = \{\infty > \lambda_1 \geq \lambda_2 \geq \dots \geq \lambda_{n-1} \geq \lambda_n \geq 0\}$. Therefore, to compute the average PEP, calculation of the joint moments of the *ordered* eigenvalues is required.

Expanding the first term in (19), which we denote by $I_1(\boldsymbol{\psi})$, we have

$$\begin{aligned} I_1(\boldsymbol{\psi}) &\triangleq \frac{1}{12} \int \dots \int_{\mathcal{D}_{ord}} \prod_m e^{-a_m \lambda_m} p(\boldsymbol{\lambda}) d\boldsymbol{\lambda} \\ &= \frac{1}{12 C_{N_t, N_r}} \sum_{p=1}^P \alpha_p \int \dots \int_{\mathcal{D}_{ord}} \prod_m e^{-(1+a_m) \lambda_m} \lambda_m^{\beta_{p,m}} d\boldsymbol{\lambda} \\ &= \frac{1}{12 C_{N_t, N_r}} \sum_{p=1}^P \alpha_p \int_0^\infty e^{-(1+a_n) \lambda_n} \lambda_n^{\beta_{p,n}} \\ &\quad \times \int_{\lambda_n}^\infty e^{-(1+a_{n-1}) \lambda_{n-1}} \lambda_{n-1}^{\beta_{p,n-1}} \times \dots \\ &\quad \times \int_{\lambda_2}^\infty e^{-(1+a_1) \lambda_1} \lambda_1^{\beta_{p,1}} d\lambda_1 \dots d\lambda_{n-1} d\lambda_n, \quad (20) \end{aligned}$$

this multiple integral will be solved sequentially. The inner integral in (20) is in the form of the upper incomplete Gamma function defined as [34, eq. 6.5.3]

$$\Gamma(a, x) = \int_x^\infty e^{-t} t^{a-1} dt. \quad (21)$$

Note that for an integer $a \geq 1$, we have

$$\Gamma(a, x) = (a-1)! e^{-x} \sum_{i=0}^{a-1} \frac{x^i}{i!}. \quad (22)$$

Hence the inner integral can be evaluated as

$$\begin{aligned} &\int_{\lambda_2}^\infty e^{-(1+a_1) \lambda_1} \lambda_1^{\beta_{p,1}} d\lambda_1 \\ &= \frac{\beta_{p,1}!}{(1+a_1)^{\beta_{p,1}+1}} e^{-(1+a_1) \lambda_2} \sum_{i_1=0}^{\beta_{p,1}} \frac{((1+a_1) \lambda_2)^{i_1}}{i_1!}. \quad (23) \end{aligned}$$

After substituting (23) into (20), it can be observed that the next integral has the structure of a series each of whose terms corresponds to an upper incomplete Gamma function. Similar forms emerge in the solution of the next integral over λ_2 . Continuing in this manner, after calculating the sequence of $(n-1)$ integrals in the form of (21), we finally have a series of integrals over λ_n each of which has the structure of the Gamma function defined as [34, eq. 6.1.1] $\Gamma(a) = \int_0^\infty e^{-t} t^{a-1} dt$; also, it is known that for an integer $a \geq 1$, $\Gamma(a) = (a-1)!$. Hence, $I_1(\boldsymbol{\psi})$ can be solved as (24), where $(x)_k = \frac{(x+k-1)!}{(x-1)!}$ denotes the rising factorial, and there are $(n-1)$ nested summations. The second term in (19), denoted by $I_2(\boldsymbol{\psi})$, can be evaluated in the same manner. Finally, the AWEP can be derived according to the union bound as [35]

$$\begin{aligned} \text{AWEP} &\leq \frac{1}{2^\eta} \sum_{\mathbf{s}} \sum_{\hat{\mathbf{s}}} \overline{\text{PEP}}(\mathbf{s}, \hat{\mathbf{s}}) \\ &\leq \frac{1}{2^\eta} \sum_{\mathbf{s}} \sum_{\hat{\mathbf{s}}} (I_1(\boldsymbol{\psi}) + I_2(\boldsymbol{\psi})). \quad (25) \end{aligned}$$

The complete expression is shown in (26).

Asymptotic Analysis

In this subsection, we will derive a high-SNR approximate expression for the AWEP, and also analyze the diversity gain of the proposed SL-MIMO system. To this end, first we define, for a vector $\boldsymbol{\psi} \neq \mathbf{0}$, a function \mathfrak{F} which counts the number of leading zeros of $\boldsymbol{\psi}$, i.e.,

$$\mathfrak{F}(\boldsymbol{\psi}) = \begin{cases} c-1 & \text{if } \psi_c \neq 0 \text{ and } \psi_m = 0 \forall m < c. \end{cases} \quad (27)$$

Next we consider the set $\mathcal{E} = \{\boldsymbol{\psi} = \mathbf{s} - \hat{\mathbf{s}} : \mathbf{s}, \hat{\mathbf{s}} \in \mathcal{S}\}$, which consists of all possible difference vectors. Define the parameter N as the maximum number of leading zeros among these vectors, i.e.,

$$N = \max_{\boldsymbol{\psi} \in \mathcal{E}} \{\mathfrak{F}(\boldsymbol{\psi})\}, \quad (28)$$

and the corresponding set $\mathcal{E}_N \subset \mathcal{E}$ as

$$\mathcal{E}_N = \{\boldsymbol{\psi} \in \mathcal{E} : \mathfrak{F}(\boldsymbol{\psi}) = N\}. \quad (29)$$

Note that N can equivalently be defined as the maximal number of leading zeros among all columns of the SL matrix \mathbf{A} , i.e., $N = \max_{l \in [L]} \{\mathfrak{F}(\mathbf{a}_l)\}$, where \mathbf{a}_l denotes the l -th column of \mathbf{A} . To see this, first we note that the codebook design

$$I_1(\boldsymbol{\psi}) = \frac{1}{12C_{N_t, N_r}} \sum_{p=1}^P \left(\alpha_p(1)_{\beta_{p,1}} \frac{1}{(1+a_1)^{\beta_{p,1}+1}} \sum_{i_1=0}^{\beta_{p,1}} \left((i_1+1)_{\beta_{p,2}} \frac{(1+a_1)^{i_1}}{(2+a_1+a_2)^{\beta_{p,2}+i_1+1}} \sum_{i_2=0}^{\beta_{p,2}+i_1} \left((i_2+1)_{\beta_{p,3}} \right. \right. \right. \\ \left. \left. \left. \times \frac{(2+a_1+a_2)^{i_2}}{(3+a_1+a_2+a_3)^{\beta_{p,3}+i_2+1}} \cdots \sum_{i_{n-1}=0}^{\beta_{p,n-1}+i_{n-2}} \left((i_{n-1}+1)_{\beta_{p,n}} \times \frac{(n-1+a_1+\cdots+a_{n-1})^{i_{n-1}}}{(n+a_1+\cdots+a_n)^{\beta_{p,n}+i_{n-1}+1}} \right) \right) \right) \right). \quad (24)$$

$$\text{AWEP} \leq \frac{1}{2^n C_{N_t, N_r}} \sum_{\mathbf{s}} \sum_{\hat{\mathbf{s}}} \sum_{p=1}^P \alpha_p \left[\left(\frac{1}{12} \frac{(1)_{\beta_{p,1}}}{(1+a_1)^{\beta_{p,1}+1}} \sum_{i_1=0}^{\beta_{p,1}} \frac{(i_1+1)_{\beta_{p,2}} (1+a_1)^{i_1}}{(2+a_1+a_2)^{\beta_{p,2}+i_1+1}} \right. \right. \\ \left. \left. \times \sum_{i_2=0}^{\beta_{p,2}+i_1} \frac{(i_2+1)_{\beta_{p,3}} (2+a_1+a_2)^{i_2}}{(3+a_1+a_2+a_3)^{\beta_{p,3}+i_2+1}} \cdots \sum_{i_{n-1}=0}^{\beta_{p,n-1}+i_{n-2}} \frac{(i_{n-1}+1)_{\beta_{p,n}} (n-1+a_1+\cdots+a_{n-1})^{i_{n-1}}}{(n+a_1+\cdots+a_n)^{\beta_{p,n}+i_{n-1}+1}} \right) \right. \\ \left. + \left(\frac{1}{4} \frac{(1)_{\beta_{p,1}}}{(1+b_1)^{\beta_{p,1}+1}} \sum_{i_1=0}^{\beta_{p,1}} \frac{(i_1+1)_{\beta_{p,2}} (1+b_1)^{i_1}}{(2+b_1+b_2)^{\beta_{p,2}+i_1+1}} \sum_{i_2=0}^{\beta_{p,2}+i_1} \frac{(i_2+1)_{\beta_{p,3}} (2+b_1+b_2)^{i_2}}{(3+b_1+b_2+b_3)^{\beta_{p,3}+i_2+1}} \cdots \right. \right. \\ \left. \left. \times \sum_{i_{n-1}=0}^{\beta_{p,n-1}+i_{n-2}} \frac{(i_{n-1}+1)_{\beta_{p,n}} (n-1+b_1+\cdots+b_{n-1})^{i_{n-1}}}{(n+b_1+\cdots+b_n)^{\beta_{p,n}+i_{n-1}+1}} \right) \right]. \quad (26)$$

condition (6) implies that for any $\mathbf{s}, \hat{\mathbf{s}} \in \mathcal{S}$ with $\mathbf{s} = \sum_{l=1}^L \mathbf{s}_l$ and for each $p \in \{1, 2, \dots, P\}$ we have and $\hat{\mathbf{s}} = \sum_{l=1}^L \hat{\mathbf{s}}_l$ and $\mathbf{s} \neq \hat{\mathbf{s}}$, for every m we have

$$s_m - \hat{s}_m = 0 \quad \text{only if} \quad \mathbf{s}_l = \hat{\mathbf{s}}_l \quad \forall l \in \mathcal{D}_m.$$

$$B_p^{(N)} = \sum_{j=N+1}^n \beta_{p,j}.$$

Therefore, (27) can be restated as

$$\mathfrak{F}(\boldsymbol{\psi}) = \mathfrak{F}(\mathbf{s} - \hat{\mathbf{s}}) = \begin{cases} c-1 & \text{if } \mathbf{s}_l = \hat{\mathbf{s}}_l \quad \forall l \in \mathcal{D}_m, \quad m < c \text{ and } \exists l \in \mathcal{D}_c \text{ such that } \mathbf{s}_l \neq \hat{\mathbf{s}}_l. \end{cases}$$

Next, observe that the maximum in (28) is attained by pairs of vectors $(\mathbf{s}, \hat{\mathbf{s}})$ that satisfy $\mathbf{s}_l = \hat{\mathbf{s}}_l$ for all l such that $\mathfrak{F}(\mathbf{a}_l) < N$. It follows that $\max_{l \in [L]} \mathfrak{F}(\mathbf{a}_l) = \max_{\boldsymbol{\psi} \in \mathcal{E}} \mathfrak{F}(\boldsymbol{\psi}) = N$. As an illustrative example, note that for the SL matrix given by (3), we have $N = 2$ since the sixth column of \mathbf{A} has 2 leading zeros and this is the maximum number of leading zeros over all columns of \mathbf{A} .

Next we provide a high-SNR approximation to the AWEP, which is based on the fact that at high SNR, the AWEP in (26) is dominated by terms corresponding to vectors in \mathcal{E}_N .

Theorem 1. *A high-SNR approximation to the AWEP for the SL-MIMO system is given by*

$$\widetilde{\text{AWEP}} \approx \frac{1}{2^n} \sum_{\mathcal{E}_N} \left(\tilde{I}_1(\boldsymbol{\psi}) + \tilde{I}_2(\boldsymbol{\psi}) \right), \quad (30)$$

where $\tilde{I}_1(\boldsymbol{\psi})$ is given by (31), and an expression for $\tilde{I}_2(\boldsymbol{\psi})$ is obtained by replacing the factor $\frac{1}{12}$ by $\frac{1}{4}$ and the coefficients a_m by b_m , for all m , in (31). Note that the set \mathcal{P}_N in (31) is defined by

$$\mathcal{P}_N = \left\{ p : B_p^{(N)} = B_{\min}^{(N)} \right\}, \quad (32)$$

where

$$B_{\min}^{(N)} = \min_{p \in \{1, 2, \dots, P\}} \left\{ B_p^{(N)} \right\},$$

Proof: See Appendix A. ■

From (31) we can now analyze the diversity gain of the system, which is given in the following Proposition.

Proposition 1. *The diversity gain of the SL-MIMO system is given by*

$$G_d = (N_r - N)(N_t - N). \quad (33)$$

Proof: Recalling that the values $\{a_n\}$ are proportional to the SNR, it can be noticed that the term in the second line of (31) is the only one that does not tend to a constant value at high SNR, i.e., we have

$$\left(1 + \frac{1+a_{N+1}}{N} \right)^{-x} \rightarrow C \cdot \text{SNR}^{-x}$$

as $\text{SNR} \rightarrow \infty$, where C is independent of the SNR. The exponent x thus gives the diversity order of the system. Considering the set \mathcal{P}_N , it can be deduced that the diversity gain of the system is given by

$$G_d = \min_p \left\{ \sum_{j=N+1}^n \beta_{p,j} \right\} + n - N. \quad (34)$$

$$\begin{aligned}
\tilde{I}_1(\psi) &\triangleq \frac{1}{12C_{N_t, N_r}} \sum_{p \in \mathcal{P}_N} \frac{\alpha_p(1) \beta_{p,1}(1) \beta_{p, N+1}}{2^{\beta_{p,3} + \dots + \beta_{p,n} + n - 2} \times \left(1 + \frac{1}{2}\right)^{\beta_{p,4} + \dots + \beta_{p,n} + n - 3} \times \dots \times \left(1 + \frac{1}{N-1}\right)^{\beta_{p, N+1} + \dots + \beta_{p,n} + n - N}} \\
&\times \frac{1}{\left(1 + \frac{1+a_{N+1}}{N}\right)^{\beta_{p, N+1} + \dots + \beta_{p,n} + n - N}} \\
&\times \frac{1}{\left(1 + \frac{1+a_{N+2}}{N+1+a_{N+1}}\right)^{\beta_{p, N+3} + \dots + \beta_{p,n} + n - N - 2} \dots \left(1 + \frac{1+a_{n-1}}{n-2+a_{N+1} + \dots + a_{n-2}}\right)^{\beta_{p, n+1}}} \\
&\times \left(\sum_{i_1=0}^{\beta_{p,1}} \frac{(i_1+1) \beta_{p,2}}{2^{\beta_{p,2} + i_1 + 1}} \cdot \sum_{i_2=0}^{\beta_{p,2} + i_1} \frac{(i_2+1) \beta_{p,3}}{\left(1 + \frac{1}{2}\right)^{\beta_{p,3} + i_2 + 1}} \dots \sum_{i_{N-1}=0}^{\beta_{p, N-1} + i_{N-2}} \frac{(i_{N-1}+1) \beta_{p, N}}{\left(1 + \frac{1}{N-1}\right)^{\beta_{p, N} + i_{N-1} + 1}} \right) \\
&\times \left(\sum_{i_{N+1}=0}^{\beta_{p, N+1}} \frac{(i_{N+1}+1) \beta_{p, N+2}}{\left(1 + \frac{1+a_{N+2}}{N+1+a_{N+1}}\right)^{\beta_{p, N+2} + i_{N+1} + 1}} \dots \sum_{i_{n-1}=0}^{\beta_{p, n-1} + i_{n-2}} \frac{(i_{n-1}+1) \beta_{p, n}}{\left(1 + \frac{1+a_n}{n-1+a_{N+1} + \dots + a_{n-1}}\right)^{\beta_{p, n} + i_{n-1} + 1}} \right). \quad (31)
\end{aligned}$$

From (16), we find that

$$\begin{aligned}
B_{\min}^{(N)} &= \min_p \left\{ \sum_{j=N+1}^n \beta_{p,j} \right\} = \sum_{j=0}^{n-N-1} (|N_t - N_r| + 2j) \\
&= (n - N) |N_t - N_r| + (n - N)(n - N - 1). \quad (35)
\end{aligned}$$

Substituting (35) into (34) we obtain (33). ■

Note that the diversity gain of the SL-MIMO system is determined by the number of transmit and receive antennas, and also by the structure of the SL matrix \mathbf{A} . Also, we note that for the special case of X- and Y-codes, our result for the diversity gain matches that obtained in [10], [11].

As an illustrative example, the closed-form expression for the approximate asymptotic AWEP for the example system with the SL matrix in (3) is shown in (36). This expression is valid for SL-MIMO systems with $n = 4$ and $N = 2$. For the MIMO system with $N_t = N_r = 4$, the diversity gain is therefore $G_d = 4$. It is worth noting that in this case, $p(\lambda)$ has 201 terms, i.e. $P = 201$; however, the asymptotic AWEP only involves 9 of these terms, i.e. $|\mathcal{P}_N| = 9$, with parameters shown in Table I.

TABLE I
PARAMETERS OCCURRING IN THE EXPRESSION (36) FOR THE APPROXIMATE ASYMPTOTIC AWEP OF AN SL-MIMO SYSTEM WITH $N_t = 4$, $N_r = 4$ AND $N = 2$. ONLY THE TERMS FOR $p \in \mathcal{P}_N$ ARE INVOLVED (HERE $|\mathcal{P}_N| = 9$).

$C_{N_t, N_r} = 144$, $B_{\min}^{(2)} = \beta_{p,3} + \beta_{p,4} = 2$				
α_p	$\beta_{p,1}$	$\beta_{p,2}$	$\beta_{p,3}$	$\beta_{p,4}$
1	6	4	2	0
-2	6	4	1	1
1	6	4	0	2
-2	5	5	2	0
4	5	5	1	1
-2	5	5	0	2
1	4	6	2	0
-2	4	6	1	1
1	4	6	0	2

IV. CODEBOOK DESIGN

In the proposed SL-MIMO system, the codebook \mathcal{S}_l for each layer l is sparsely spread over a subset of the eigen-channels. Therefore, designing appropriate codebooks \mathcal{S}_l , as well as a good sparse layering matrix \mathbf{A} , can significantly improve the error rate performance of the system. In the following, we focus on codebook optimization with a view to minimizing the average word error probability of the system.

It is well-known [36] that the average error probability at high SNR can be approximated as

$$\text{AWEP} \approx (G_c \bar{\gamma})^{-G_d}, \quad (37)$$

where $\bar{\gamma}$ is the average SNR, and G_c and G_d are the *coding gain* and *diversity gain*, respectively. As shown in (33), G_d depends on the MIMO configuration and the SL matrix \mathbf{A} , and from (30), it can be inferred that G_c depends on the set \mathcal{E}_N . It is well-known that for an $N_t \times N_r$ MIMO system, the maximum achievable diversity gain is $N_t N_r$. In the SL-MIMO system, this maximum can be attained when all layers share the strongest eigen-channel, i.e., $N = 0$. In other words, in a fixed-rate system, there is a trade-off between diversity gain and coding gain, as sharing the strongest eigen-channel among all layers results in smaller Euclidean distances and thus a lower coding gain. Therefore, the desired design goal can be defined by the optimization problem

$$(\mathbf{A}^*, \{\bar{\mathcal{S}}_l^*\}) = \arg \min_{\mathbf{A}, \{\bar{\mathcal{S}}_l\}} \text{AWEP}_{\text{ub}}(\mathbf{A}, \{\bar{\mathcal{S}}_l\}), \quad (38)$$

where $(\mathbf{A}^*, \{\bar{\mathcal{S}}_l^*\})$ denotes the jointly optimum values of the SL matrix \mathbf{A} and the *shortened codebooks* (i.e., multidimensional constellations) $\{\bar{\mathcal{S}}_l\}$, where $\bar{\mathcal{S}}_l$ is the n_l -dimensional constellation obtained when we restrict \mathcal{S}_l to the index set \mathcal{N}_l (i.e., excluding dimensions with zero values from these vectors), and AWEP_{ub} denotes the upper bound on the AWEP given by (26). The joint optimization in (38) is prohibitively complex to implement, even for a small constellation size and a very limited number of layers and antennas. Therefore,

$$\begin{aligned} \widetilde{\text{AWEP}} \approx & \frac{1}{2^\eta} \sum_{\mathcal{E}_N} \left(\left[\frac{1}{12C_{N_t, N_r}} \sum_{p \in \mathcal{P}_N} \frac{\alpha_p(1)_{\beta_{p,1}}(1)_{\beta_{p,3}}}{2^{\beta_{p,3} + \beta_{p,4} + 2} \left(1 + \frac{1+a_3}{2}\right)^{\beta_{p,3} + \beta_{p,4} + 2}} \left(\sum_{i_1=0}^{\beta_{p,1}} \frac{(i_1+1)_{\beta_{p,2}}}{2^{\beta_{p,2} + i_1 + 1}} \right) \left(\sum_{i_3=0}^{\beta_{p,3}} \frac{(i_3+1)_{\beta_{p,4}}}{\left(1 + \frac{1+a_4}{3+a_3}\right)^{\beta_{p,4} + i_3 + 1}} \right) \right] \right. \\ & \left. + \left[\frac{1}{4C_{N_t, N_r}} \sum_{p \in \mathcal{P}_N} \frac{\alpha_p(1)_{\beta_{p,1}}(1)_{\beta_{p,3}}}{2^{\beta_{p,3} + \beta_{p,4} + 2} \left(1 + \frac{1+b_3}{2}\right)^{\beta_{p,3} + \beta_{p,4} + 2}} \left(\sum_{i_1=0}^{\beta_{p,1}} \frac{(i_1+1)_{\beta_{p,2}}}{2^{\beta_{p,2} + i_1 + 1}} \right) \left(\sum_{i_3=0}^{\beta_{p,3}} \frac{(i_3+1)_{\beta_{p,4}}}{\left(1 + \frac{1+b_4}{3+b_3}\right)^{\beta_{p,4} + i_3 + 1}} \right) \right] \right). \end{aligned} \quad (36)$$

we adopt a more practical sub-optimal approach which is explained in the following text. First, we design (or select) an SL matrix \mathbf{A}^+ with the desired number of layers L , and then design the optimum M -ary multidimensional constellations $\{\tilde{\mathcal{S}}_l\}$ for this designed \mathbf{A}^+ . As stated earlier, the complexity of the MP detector is determined by the structure of the SL matrix. Hence, the SL matrix can be designed to target a high diversity gain, while ensuring a good sparse matrix structure for MP decoding.

Having designed the SL matrix \mathbf{A}^+ , the optimization problem is reduced to

$$\{\tilde{\mathcal{S}}_l^*\} = \arg \min_{\{\tilde{\mathcal{S}}_l\}} \text{AWEP}_{\text{ub}}(\mathbf{A}^+, \{\tilde{\mathcal{S}}_l\}), \quad (39)$$

Next, the problem is to jointly design L multidimensional constellations each having size M . It was shown in [37] that the *minimum Euclidean distance* and the *minimum product distance* of a multidimensional constellation represent the key factors affecting the error rate performance in Gaussian and Rayleigh fading channels, respectively. For this reason, most of the multidimensional constellation design techniques for SCMA systems focus on designing a *mother* constellation for the system to maximize the minimum Euclidean or product distance of a *single* user (in the SL-MIMO context, this would correspond to a single layer). A comprehensive comparison of different multidimensional constellation design methods is presented in [38]. However, in the proposed SL-MIMO system, the fading experienced in the eigen-channels corresponds to the *ordered* eigenvalues; due to this fact, and considering the role of the difference vectors ψ in (26) and (31), it can be seen that neither the Euclidean distance nor the product distance is a key factor in determining the error rate performance of SL-MIMO. On the other hand, it is clear from (15) that the *weighted Euclidean distance*, i.e., $\sum_m \lambda_m |\psi_m|^2$, has a significant effect on the performance of the SL-MIMO system. However, maximizing the weighted Euclidean distance of the constellation for a single layer is not a suitable design strategy, as this would result in dedicating the total energy of each multidimensional symbol to the strongest available eigen-channel. Therefore, we first choose a general one-dimensional² *base constellation* \mathcal{M} with unit average energy, e.g., a lattice-based constellation such as PAM or QAM, and repeat it for the other dimensions (the constellation symbol is also repeated for

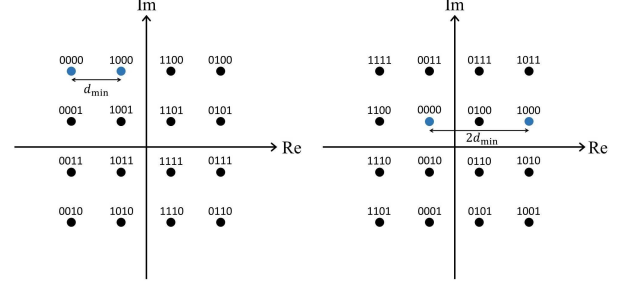


Fig. 2. An example of a 2-dimensional constellation which uses 16-QAM as the base constellation \mathcal{M} for the first dimension and a permuted version of \mathcal{M} for the second dimension. Here the permutation is performed for the real and imaginary dimensions independently. Neighboring symbols in the first dimension (eigen-channel) are separated in the other dimension (eigen-channel). This will increase the overall minimum distance.

these dimensions). In addition, permutation among dimensions can be used such that each multidimensional constellation point contains a different symbol in each dimension. This helps to increase the minimum distance³ [39]. The permutation can be done by changing the arrangement in the sequence of constellation points of the base constellation. Fig. 2 shows an example of a 2-dimensional constellation which uses a 16-QAM as the base constellation, and a permuted version is used for the other dimension. In this example, the permutation is performed in the real and imaginary dimensions independently. It can be seen that how permutation benefits the system via increasing the minimum Euclidean distance: neighboring symbols in the first dimension (eigen-channel) are separated in the other dimension (eigen-channel). Any pair of symbols with a distance of d_{\min} in one dimension has a distance of at least $2d_{\min}$ in the other dimension.

After choosing a base constellation, we design the *layer operators* that are applied to the multidimensional constellation in order to improve the error rate performance by separating the interfering symbols. Hence, the constellation for a layer l is given by

$$\tilde{\mathcal{S}}_l = \{\Delta_l \mathbf{m}_i, i = 1, 2, \dots, M\},$$

where $\Delta_l \in \mathbb{C}^{n_l \times n_l}$ is the l -th *layer operator*, and $\mathbf{m}_i \in \mathbb{C}^{n_l \times 1}$ is an n_l -dimensional symbol whose elements are in the

²Here we adopt the convention that 'dimensions' refers to *complex* dimensions, i.e., each dimension corresponds to a complex symbol.

³A similar method has been used for multidimensional constellation design in LDS and SCMA systems. Repeated M -QAM is identified as M -LDS in [17], while the permuted version was proposed in [39].

set of the base constellation \mathcal{M} (note that in repetition mode the vector \mathbf{m}_i is uniquely determined by its first element).

Layer operators are unitary matrices that rotate and scale the complex symbol to provide unique symbols for each layer. From (26) it can be seen that $\widetilde{\text{AWEP}}_{\text{ub}}$ consists of terms of the form

$$\frac{(k-1+a_1+\dots+a_{k-1})^{i_{k-1}}}{(k+a_1+\dots+a_k)^{\beta_{p,k+i_{k-1}+1}}}. \quad (40)$$

In our scheme, we perform scaling in addition to rotation, since the fading coefficients are in the ordered condition and scaling factors help to control $\widetilde{\text{AWEP}}_{\text{ub}}$ by altering the ratios in (40). Moreover, the resulting power imbalance helps the MP detector to converge faster, as reliable detection of the “stronger” symbols can aid the detector to subsequently resolve the “weaker” symbols. Hence, the layer operator is written as

$$\Delta_l = \begin{bmatrix} \rho_{1,l} e^{j\phi_{1,l}} & \dots & 0 \\ \vdots & \ddots & \vdots \\ 0 & \dots & \rho_{n_l,l} e^{j\phi_{n_l,l}} \end{bmatrix}, l = 1, \dots, L, \quad (41)$$

such that

$$\rho_{1,l}^2 + \dots + \rho_{n_l,l}^2 = E_s, \forall l, \quad (42)$$

where $0 \leq \phi_{j,l} < \pi$ for all j and l , and $\rho_{j,l} \geq 0$ for all j and l . Joint optimization of all angles and scaling factors still requires a high-dimensional exhaustive search of prohibitive complexity; therefore, to further simplify the problem, first we design sub-optimal angles $\{\phi_{j,l}^+\}$ in such a way as to maximize the minimum Euclidean distance between interfering symbols independently on each eigen-channel. Then, we proceed to optimize the scaling factors in order to minimize the error rate. This stage is also performed in multiple steps, proceeding from the layers using the weakest eigen-channels to the layers using the strongest eigen-channels, in order to reduce the complexity of the problem. Then, the optimization problem of each step of this multi-step problem can be defined as

$$\underset{\rho_{j,l}, \forall l \in \mathcal{L}_{N'}, \forall j \in [n_l]}{\text{minimize}} \quad \widetilde{\text{AWEP}}_{N'} \left(\mathbf{A}^+, \left\{ \bar{\mathfrak{S}}_l \left(\Delta_l(\rho_{j,l}, \phi_{j,l}^+) \right) \right\} \right) \quad (43)$$

subject to (42),

where $\mathcal{L}_{N'} = \{l : \mathfrak{F}(\mathbf{a}_l) = N'\}$ and $\widetilde{\text{AWEP}}_{N'}$ is the asymptotic value of the contribution to the AWEP from layers having at least N' leading zeros in their codewords. $\widetilde{\text{AWEP}}_{N'}$ can be easily derived from (30) by replacing N with N' in $\tilde{I}_1(\boldsymbol{\psi})$ and $\tilde{I}_2(\boldsymbol{\psi})$ and implementing summation over the set $\mathcal{E}_{N'} = \{\boldsymbol{\psi} \in \mathcal{E} : \mathfrak{F}(\boldsymbol{\psi}) \geq N'\}$. We begin by solving (43) for $N' = N$, i.e., $\widetilde{\text{AWEP}}_N = \widetilde{\text{AWEP}}$, and find the corresponding scaling factors $\{\rho_{j,l}\}$ by performing a grid search. This grid search operates in parallel for variables $\rho_{j,l}$ for all l that satisfy $\mathfrak{F}(\mathbf{a}_l) = N'$ and for all $j = \{1, 2, \dots, n_l\}$. For each such l , there are $n_l - 1$ independent variables due to (42), and therefore the number of variables to be optimized in parallel in this step is $\sum_{l \in \mathcal{L}_{N'}} (n_l - 1)$, which is usually manageable since the numbers n_l are relatively small. Then, in each subsequent

step, we decrement N' and solve (43) again for the next set of optimal scaling factors $\{\rho_{j,l}\}$.

At the final step we have $N' = 0$, and $\widetilde{\text{AWEP}}_0$ is equivalent to AWEP_{ub} given in (26). At this point, direct optimization of the scaling factors of the remaining layers using (26) does not represent a practical approach as the objective function is relatively complex. Therefore, recalling the expression (15) for the PEP, we maximize the minimum argument of the Q-function in (15) by implementing a search process over the layers with $\mathfrak{F}(\mathbf{a}_l) = 0$, where each eigenvalue λ_m is replaced by its average value denoted by $\bar{\lambda}_m$. This amounts to maximizing the minimum *weighted Euclidean distance* between pairs of symbols, $\sum_m \bar{\lambda}_m |\psi_m|^2$, where $\{\bar{\lambda}_m\}$ can be derived analytically from the MGF calculated in the previous section.⁴

Design Procedure

In this subsection, we briefly summarize the above design procedure in steps for a generic SL-MIMO system. First, an appropriate sparse SL matrix \mathbf{A} is chosen, taking into account the complexity of the MP detector and the desired number of layers. Then, we choose a general M -ary one-dimensional *base constellation* \mathcal{M} with unit average energy. This base constellation is repeated (or permuted) over the other dimensions to produce a generic multidimensional constellation for the SL-MIMO system. After choosing the SL matrix and constellation, the optimization of the layer operators in (41) can be performed using the following steps.

Step 1: We find the angles $\{\phi_{j,l}\}$ in such a way as to maximize the minimum Euclidean distance between interfering symbols independently on each eigen-channel. Consider the m -th row of \mathbf{A} , and note that this row has row weight d_m , i.e., d_m layers share eigen-channel m . As was shown in [40], the optimum rotation angles for M -PSK constellation are given by

$$\phi_{j,l} = \frac{k}{d_m} \left(\frac{2\pi}{M} \right), \quad k = 0, \dots, d_m - 1, \quad (44)$$

and therefore this set of rotation angles will be assigned to the set of interfering symbols.

Step 2 to end: We solve the optimization problem in (43) for $N' = N, N - 1, \dots, 1, 0$. In each step, we find the optimal $\rho_{j,l}$ for all l that satisfy $\mathfrak{F}(\mathbf{a}_l) = N'$ and for all $j = \{1, 2, \dots, n_l\}$. Note that in the final step when $N' = 0$ (and also possibly in preceding steps), since the objective function in (43) is relatively complex, we can instead choose to maximize the minimum *weighted Euclidean distance* between pairs of symbols, i.e.,

$$\underset{\rho_{j,l}, \forall l \in \mathcal{L}_{N'}, \forall j \in [n_l]}{\text{maximize}} \left\{ \min_{\boldsymbol{\psi} \in \mathcal{E}_{N'}} \left\{ \sum_m \bar{\lambda}_m |\psi_m|^2 \right\} \right\}.$$

To elucidate this procedure, we next briefly describe the steps for the design example for the case where the SL matrix is given in (3), and where the base constellation \mathcal{M} is a 4-QAM (QPSK) constellation.

⁴Although this optimization procedure can still have quite a high complexity for large MIMO systems and high-order base constellations \mathcal{M} , it needs to be performed only once and can be deployed offline.

Step 1: Consider rows of \mathbf{A} , 3 layers share each of the eigen-channels. Considering (44), the optimum rotation angles are $\phi_{j,l}^+ \in \{0, \frac{\pi}{6}, \frac{\pi}{3}\}$; at each eigen-channel, this set of three rotation angles will be assigned to the set of three interfering symbols.

Step 2: Next, the optimization sub-problem is to minimize $\widetilde{\text{AWEP}}$ in (36) by searching over all possible difference vectors for layer 6 and find the sub-optimal $\rho_{1,6}^+$ and $\rho_{2,6}^+$. Via this method, the design of Δ_6 (and thus \mathcal{S}_6) is achieved. This will be used as the constellation for layer 6 in the next steps.

Step 3: In this step, it is first required to find $\widetilde{\text{AWEP}}_1$ as the objective function. This can be found in a way similar to that of the asymptotic AWE. Referring to (43), here our optimization is targeting the layers that satisfy $\mathfrak{F}(\mathbf{a}_l) = 1$, i.e., layers 4 and 5. Therefore, in this step we obtain the scaling parameters jointly for layers 4 and 5.

Step 4: Finally, $N' = 0$, i.e. the objective function is the upper bound of AWE given in (26), and layers 1, 2 and 3 meet the condition $\mathfrak{F}(\mathbf{a}_l) = 0$. However, instead of solving the problem in (43), in this step we maximize the minimum *weighted Euclidean distance* by searching over all possible difference vectors in order to find the optimal scaling parameters of Δ_1 , Δ_2 and Δ_3 .

V. NUMERICAL RESULTS

In this section, we demonstrate the performance of the proposed SL-MIMO system design using numerical simulations. Fig. 3 shows the AWE performance of the SL-MIMO system with $N_t = 4$, $N_r = 4$, $M = 4$, $L = 6$, and SL matrix given by (3). The SL-MIMO constellations have been optimized as described in Section IV. For each codebook, a 4-QAM constellation is used as the base constellation and is only repeated (not permuted) over the second eigen-channel. The figure provides a comparison with a similar SL-MIMO system where each layer uses a rotated QAM constellation. It can be observed that the optimized constellations provide a 2.3 dB improvement at an AWE of 10^{-4} . The analytical (equation (26)) and asymptotic (equation (36)) results are also included in this figure, which verifies the correctness of the simulation results and also the tightness of the analytical AWE upper bound. The asymptotic curves in Fig. 3 verify that the diversity gain of the system is equal to 4, in accordance with Proposition 1 (here $N_t = N_r = 4$ and $N = 2$). In addition, the results are shown for both the ML and MP detection methods. Here 5 iterations were used in the MP detector, as this was found to produce a negligible performance degradation with respect to ML detection, which is shown in Fig. 4. This figure presents the AWE performance of the MP detector versus the number of iterations of message passing, at an SNR of 20 dB. It can be seen that the MP detector converges to an AWE value that is very close to that of the ML detector within a very small number of iterations; hence, from this point onwards, we only plot the performance of the MP detector.

Next we compare the AWE of the proposed SL-MIMO system (with optimized constellations) with that of X- and Y-codes [11], which serve as the benchmark schemes for the

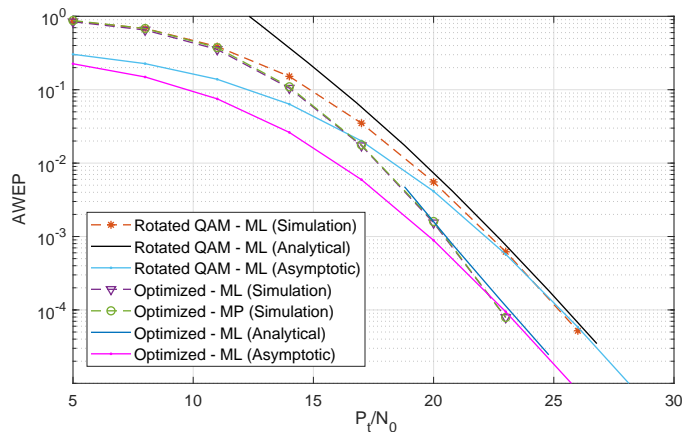


Fig. 3. Illustration of the benefits of the proposed constellation design method for SL-MIMO. The performance of the SL-MIMO system with the proposed (optimized) constellations is compared to that of SL-MIMO with rotated QAM on each layer. Here $N_t = N_r = 4$, $L = 6$ and $M = 4$.

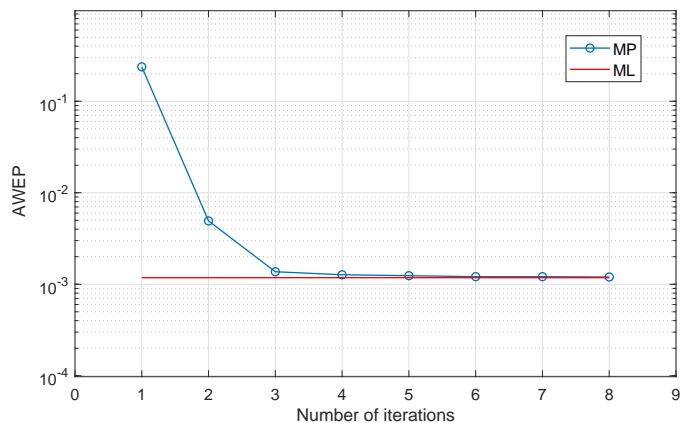


Fig. 4. Convergence behavior of the MP detector for the SL-MIMO system. Here the SL matrix \mathbf{A} is given by (3), $N_t = N_r = 4$, $M = 4$ and $P_t/N_0 = 20$ dB.

proposed approach. It was shown in [11] that X- and Y-codes perform better than other competing schemes in this context such as the $E-d_{\min}$ scheme proposed in [10] (for more details, we refer the readers to [11] and references therein). A key advantage of our proposed SL-MIMO scheme is that the system can be *overloaded*; however, in order to have a fair comparison, we choose $L = n$, i.e., the number of layers is equal to the number of available eigen-channels, similar to the case of X- and Y-codes.

In Fig. 5, we compare the AWE performance of the proposed SL-MIMO system with $L = 4$ with that of X- and Y-codes for $M = 4, 16$ and 64 . We use

$$\mathbf{A}_1 = \begin{bmatrix} 1 & 1 & 1 & 0 \\ 1 & 0 & 0 & 1 \\ 0 & 1 & 0 & 1 \\ 0 & 0 & 1 & 0 \end{bmatrix}$$

as the SL matrix for $M = 4$ and $M = 16$, where 4-QAM and 16-QAM are used as the base constellations, respectively, and

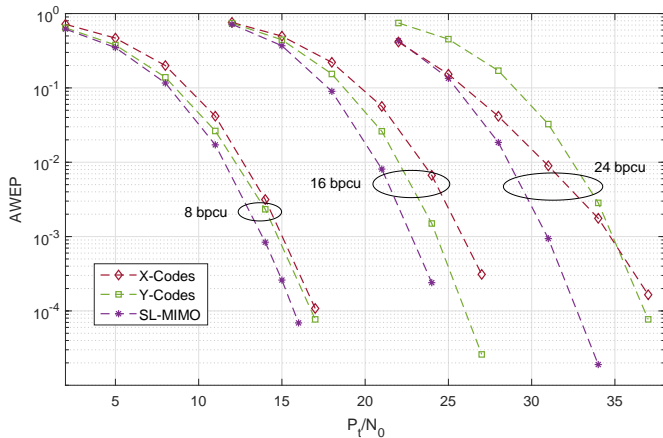


Fig. 5. Comparison of the AWEP performance of the proposed SL-MIMO system with that of X- and Y-codes for $M = 4, 16$ and 64 and $N_t = N_r = 4$.

we use the matrix

$$\mathbf{A}_2 = \begin{bmatrix} 1 & 1 & 0 & 0 \\ 0 & 0 & 1 & 1 \\ 1 & 0 & 0 & 1 \\ 0 & 1 & 1 & 0 \end{bmatrix}$$

for the SL-MIMO system with $M = 64$, where 8-PAM is used as the base constellation for the real and imaginary parts of each data symbol. For each SL-MIMO system, the constellations are optimized as described in Section IV. The results show that the performance of the SL-MIMO system is superior to that of X- and Y-codes in all scenarios, and this performance improvement increases dramatically at higher data rates. This is mainly due to the fact that in SL-MIMO, a layer interferes with different layers through its eigen-channels, and the resulting *interference diversity* benefits the system. The gain over X-codes is approximately 1.2 dB, 2.5 dB and 4.9 dB at 8 bpcu, 16 bpcu and 24 bpcu systems, respectively, at an AWEP of 10^{-4} . The proposed system also achieves 1 dB, 1.2 dB and 3.2 dB performance improvement over Y-codes at 8 bpcu, 16 bpcu and 24 bpcu, respectively. As noted in [11], we can observe that for low data rates, Y-codes exhibit a performance improvement over X-codes at all SNR, since they perform power and rate allocation within a pair of layers and eigen-channels; at higher data rates, however, the performance diminishes significantly, as instead of using n layers each having M constellation points, the transmitter for Y-codes creates $\frac{n}{2}$ layers each having M^2 constellation points. In fact, an M^2 -QAM symbol is transmitted by the stronger eigen-channel on each pair and a 2-bit coded version of that symbol is transmitted through the weaker eigen-channel, resulting in a large number of difference vectors with small Euclidean distances, and therefore poor performance at low and medium SNRs. In addition, the performance of the X-codes becomes worse at higher data rates, as the Euclidean distances between interfering QAM symbols are more sensitive to rotation angles at higher data rates. This results in Euclidean distances which become close to zero in the medium SNR range, which in turn causes a decrease in the diversity gain.

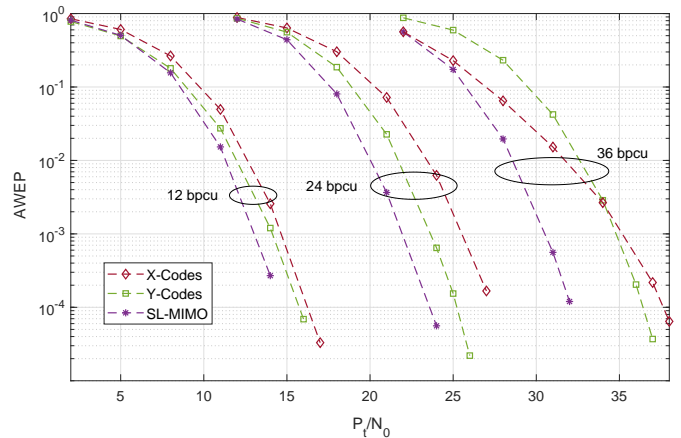


Fig. 6. Comparison of the AWEP performance of the proposed SL-MIMO system with that of X- and Y-codes for $M = 4, 16$ and 64 and $N_t = N_r = 6$.

It is worth mentioning that the complexity of the MP detector is $\mathcal{O}(M^3)$ in the case when \mathbf{A}_1 is used. However, the complexity of the receiver and optimization process is reduced by using the matrix \mathbf{A}_2 for the SL-MIMO system with $M = 64$. In addition to this, instead of optimizing the rotation angles in *Step 1*, we set $\phi_{j,l} = 0$ in order to obtain *real-valued* Δ_l . This further reduces the complexity of the receiver by separating the real and imaginary parts of the data symbols and using two \sqrt{M} -PAM constellations together with application of two independent detectors at the receiver on the real and imaginary parts of the received signal. Hence, the complexity of the receiver in this case is $\mathcal{O}(M)$, similar to the case of X-codes.

Fig. 6 compares the performance of the SL-MIMO system with X- and Y-codes in a 6×6 MIMO system, i.e., $N_t = N_r = 6$. Similar to the 4×4 system, we use two different SL matrices,

$$\mathbf{A}_3 = \begin{bmatrix} 1 & 1 & 1 & 0 & 0 & 0 \\ 0 & 0 & 0 & 1 & 1 & 1 \\ 0 & 0 & 1 & 0 & 0 & 1 \\ 0 & 1 & 0 & 0 & 1 & 0 \\ 1 & 0 & 0 & 1 & 0 & 0 \\ 0 & 0 & 0 & 0 & 0 & 0 \end{bmatrix}, \mathbf{A}_4 = \begin{bmatrix} 1 & 1 & 0 & 0 & 0 & 0 \\ 0 & 0 & 1 & 1 & 0 & 0 \\ 0 & 0 & 0 & 0 & 1 & 1 \\ 0 & 0 & 0 & 1 & 1 & 0 \\ 0 & 1 & 1 & 0 & 0 & 0 \\ 1 & 0 & 0 & 0 & 0 & 1 \end{bmatrix}, \quad (45)$$

\mathbf{A}_3 for $M = 4$ and 16 , and \mathbf{A}_4 for $M = 64$. Similar to the 4×4 system, we use 4- and 16-QAM constellations for the cases where $M = 4$ and $M = 16$, respectively, and for the system with $M = 64$, 8-PAM is used as the base constellation per real dimension. As expected, the SL-MIMO system achieves even higher gains in a larger MIMO system. The constellation-optimized SL-MIMO designs provide 1.6 dB, 3.7 dB and 5.6 dB improvement over X-codes and 1.2 dB, 1.7 dB and 4.7 dB gain over Y-codes at 12 bpcu, 24 bpcu and 36 bpcu systems, respectively, at an AWEP of 10^{-4} . Recalling (45), the complexity of the MP detector in the 6×6 system is similar to that of the 4×4 system. It can be seen that in \mathbf{A}_3 , 3 layers are interfering at eigen-channels 1 and 2, therefore $d_{\max} = 3$ and thus, the complexity of the receiver is $\mathcal{O}(M^3)$. However, in the matrix \mathbf{A}_4 , each eigen-channel is shared between 2 layers, and since $\phi_{j,l} = 0$, and consequently the real and imaginary parts of data symbols are separated, thus the complexity of

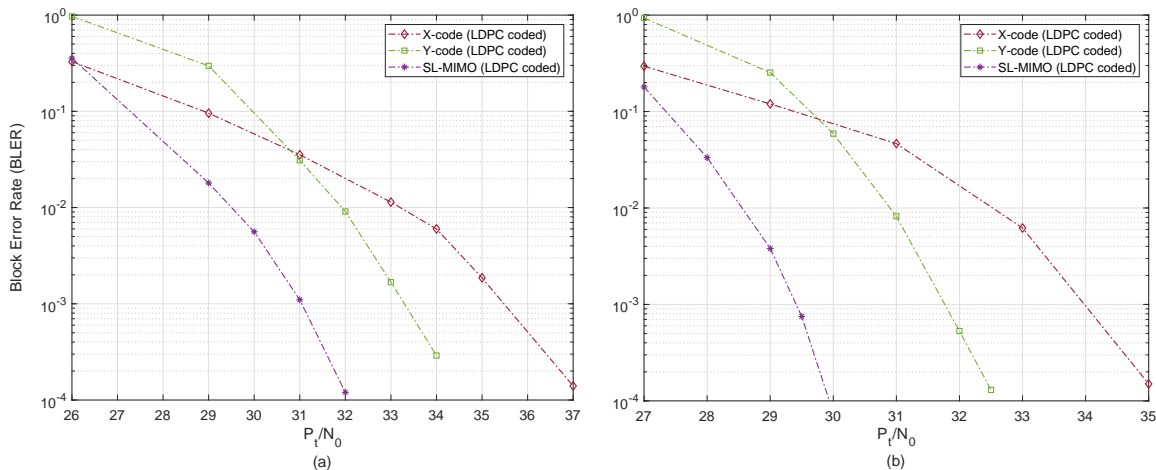


Fig. 7. Comparison of the average BLER performance of the proposed SL-MIMO system with that of X- and Y-codes for $M = 64$, where an LDPC code is used with rate 0.47. (a) $N_t = N_r = 4$, (b) $N_t = N_r = 6$.

the receiver is $\mathcal{O}(M)$.

In Fig. 7, we compare the error rate performance of SL-MIMO systems and X- and Y-codes in the presence of channel coding. Here we apply the LDPC code with code rate 0.47 that has been implemented in the 5G New Radio (NR) standard [41], and the constellation size is $M = 64$. The results show that the proposed SL-MIMO scheme remains dominant in error rate performance over X- and Y-codes when channel coding is implemented in the considered system. The gain over X-codes is 5 dB and 5.5 dB, and the gain over Y-codes is 2.5 dB and 2.8 dB in 4×4 and 6×6 MIMO systems, respectively, at an average block error rate (BLER) of 10^{-4} . We also observe that the resulting enhancement is increasing with an increase in the SNR.

VI. CONCLUSION

In this paper, we proposed the SL-MIMO transmission technique, which improves the error rate performance of MIMO systems and thereby provides excellent performance in both diversity order and coding gain. In SL-MIMO, code-domain non-orthogonal transmission and SVD precoding are combined to allow re-use of eigen-channels. At the receiver, a low-complexity MP detector can be applied which has performance close to that of ML detection. We evaluated the error rate performance of the SL-MIMO system by calculating the joint MGF of the *ordered* eigenvalues. A closed-form upper bound on the AWEF and asymptotic AWEF were derived and the diversity gain of the system was analytically obtained. Based on these analytical results, an optimization procedure was introduced to design sparse layering codebooks to minimize the error rate of the SL-MIMO system. The error rate performance of the SL-MIMO system has been compared with that of X- and Y-codes by numerical simulations. The results have shown that the performance of the SL-MIMO system outperforms other competing schemes in all of the considered scenarios. This enhancement becomes more prominent at higher data rates and in larger MIMO systems. An interesting direction of future research along this line is that of extension of the SL-MIMO scheme to a *multiuser* uplink

communication scenario, where users play the role of layers, and in particular the development of suitable low-complexity message-passing detection algorithms for the multiuser SL-MIMO setting.

APPENDIX A PROOF OF THEOREM 1

To prove (31), we rewrite (24) in the equivalent form of (46), which (with some minor manipulation) can be re-expressed as (47).

It can be seen in (47) that there are terms of the form

$$\left(1 + \frac{1 + a_k}{k - 1 + a_1 + \dots + a_{k-1}}\right)^{-c_{p,k}}$$

in the first line with $k = 2, \dots, n - 1$ and $c_{p,k} = \beta_{p,k+1} + \dots + \beta_{p,n} + n - k$, and in the nested sum in the second line with $k = 2, \dots, n$ and $c_{p,k} = \beta_{p,k} + i_{k-1} + 1$. For a difference vector ψ which has no nonzero entries, each of these terms tends to a constant at high SNR, and only the term $(1 + a_1)^{-(\beta_{p,1} + \dots + \beta_{p,n} + n)}$ in line 1 varies with SNR. However, for a difference vector ψ with $\mathfrak{F}(\psi) = m > 0$ (i.e., $a_1 = \dots = a_m = 0$), only the term with $k = m + 1$, i.e. $\left(1 + \frac{1 + a_{m+1}}{m}\right)^{-c_p}$, where $c_p = \beta_{p,m+1} + \dots + \beta_{p,n} + n - m + i_m$, varies at high SNR. In addition, for each p , the minimum value of c_p among all vectors $\psi \in \mathcal{E}$ corresponds to the maximum value of m , which is equal to N . Hence, it can be deduced that vectors $\psi \in \mathcal{E}_N$ provide terms that dominate the high-SNR value of the AWEF. As a consequence, to obtain the approximate AWEF, we set $\psi_1 = \dots = \psi_N = 0$, or equivalently $a_1 = \dots = a_N = 0$, in equation (47); after this we obtain (48).

From (48), we can observe that the terms in line 2 and 5 are constants, and the terms in line 4 and the nested sum in line 7 also tend to constants which depend on the value of the vector ψ . In addition, the terms of the sum in line 6 are of the form

$$(\omega_1 + \omega_2 \text{SNR})^{-\delta},$$

$$\begin{aligned}
I_1(\psi) &= \frac{1}{12C_{N_t, N_r}} \sum_{p=1}^P \frac{\alpha_p(1)_{\beta_{p,1}}}{(1+a_1)^{\beta_{p,1}+1}} \times \frac{1}{(1+a_1)^{\beta_{p,2}+1} (2+a_1+a_2)^{\beta_{p,3}+1} \dots (n-1+a_1+\dots+a_{n-1})^{\beta_{p,n}+1}} \\
&\times \sum_{i_1=0}^{\beta_{p,1}} \frac{(i_1+1)_{\beta_{p,2}}}{\left(1+\frac{1+a_2}{1+a_1}\right)^{\beta_{p,2}+i_1+1}} \sum_{i_2=0}^{\beta_{p,2}+i_1} \frac{(i_2+1)_{\beta_{p,3}}}{\left(1+\frac{1+a_3}{2+a_1+a_2}\right)^{\beta_{p,3}+i_2+1}} \dots \sum_{i_{n-1}=0}^{\beta_{p,n-1}+i_{n-2}} \frac{(i_{n-1}+1)_{\beta_{p,n}}}{\left(1+\frac{1+a_n}{n-1+a_1+\dots+a_{n-1}}\right)^{\beta_{p,n}+i_{n-1}+1}}.
\end{aligned} \tag{46}$$

$$\begin{aligned}
I_1(\psi) &= \frac{1}{12C_{N_t, N_r}} \sum_{p=1}^P \frac{\alpha_p(1)_{\beta_{p,1}}}{(1+a_1)^{\beta_{p,1}+\dots+\beta_{p,n}+n} \left(1+\frac{1+a_2}{1+a_1}\right)^{\beta_{p,3}+\dots+\beta_{p,n}+n-2} \dots \left(1+\frac{1+a_{n-1}}{n-2+a_1+\dots+a_{n-2}}\right)^{\beta_{p,n}+1}} \\
&\times \sum_{i_1=0}^{\beta_{p,1}} \frac{(i_1+1)_{\beta_{p,2}}}{\left(1+\frac{1+a_2}{1+a_1}\right)^{\beta_{p,2}+i_1+1}} \sum_{i_2=0}^{\beta_{p,2}+i_1} \frac{(i_2+1)_{\beta_{p,3}}}{\left(1+\frac{1+a_3}{2+a_1+a_2}\right)^{\beta_{p,3}+i_2+1}} \dots \sum_{i_{n-1}=0}^{\beta_{p,n-1}+i_{n-2}} \frac{(i_{n-1}+1)_{\beta_{p,n}}}{\left(1+\frac{1+a_n}{n-1+a_1+\dots+a_{n-1}}\right)^{\beta_{p,n}+i_{n-1}+1}}.
\end{aligned} \tag{47}$$

$$\begin{aligned}
I_1(\psi|\psi_1 = \dots = \psi_N = 0) &= \\
&\frac{1}{12C_{N_t, N_r}} \sum_{p=1}^P \frac{\alpha_p(1)_{\beta_{p,1}}}{2^{\beta_{p,3}+\dots+\beta_{p,n}+n-2} \times \left(1+\frac{1}{2}\right)^{\beta_{p,4}+\dots+\beta_{p,n}+n-3} \times \dots \times \left(1+\frac{1}{N-1}\right)^{\beta_{p,N+1}+\dots+\beta_{p,n}+n-N}} \\
&\times \frac{1}{\left(1+\frac{1+a_{N+1}}{N}\right)^{\beta_{p,N+2}+\dots+\beta_{p,n}+n-N-1}} \\
&\times \frac{1}{\left(1+\frac{1+a_{N+2}}{N+1+a_{N+1}}\right)^{\beta_{p,N+3}+\dots+\beta_{p,n}+n-N-2} \dots \left(1+\frac{1+a_{n-1}}{n-2+a_{N+1}+\dots+a_{n-2}}\right)^{\beta_{p,n}+1}} \\
&\times \sum_{i_1=0}^{\beta_{p,1}} \frac{(i_1+1)_{\beta_{p,2}}}{2^{\beta_{p,2}+i_1+1}} \sum_{i_2=0}^{\beta_{p,2}+i_1} \frac{(i_2+1)_{\beta_{p,3}}}{\left(1+\frac{1}{2}\right)^{\beta_{p,3}+i_2+1}} \dots \sum_{i_{N-1}=0}^{\beta_{p,N-1}+i_{N-2}} \frac{(i_{N-1}+1)_{\beta_{p,N}}}{\left(1+\frac{1}{N-1}\right)^{\beta_{p,N}+i_{N-1}+1}} \\
&\times \sum_{i_N=0}^{\beta_{p,N}+i_{N-1}} \frac{(i_N+1)_{\beta_{p,N+1}}}{\left(1+\frac{1+a_{N+1}}{N}\right)^{\beta_{p,N+1}+i_N+1}} \\
&\times \sum_{i_{N+1}=0}^{\beta_{p,N+1}+i_N} \frac{(i_{N+1}+1)_{\beta_{p,N+2}}}{\left(1+\frac{1+a_{N+2}}{N+1+a_{N+1}}\right)^{\beta_{p,N+2}+i_{N+1}+1}} \dots \sum_{i_{n-1}=0}^{\beta_{p,n-1}+i_{n-2}} \frac{(i_{n-1}+1)_{\beta_{p,n}}}{\left(1+\frac{1+a_n}{n-1+a_{N+1}+\dots+a_{n-1}}\right)^{\beta_{p,n}+i_{n-1}+1}}.
\end{aligned} \tag{48}$$

where $\delta = \beta_{p,N+1} + i_N + 1$. At high-SNR values, the sum can be approximated by the term with the largest exponent (smallest δ), which corresponds to the term with $i_N = 0$. Hence, it can be concluded that

$$\begin{aligned}
&\sum_{i_N=0}^{\beta_{p,N}+i_{N-1}} \frac{(i_N+1)_{\beta_{p,N+1}}}{\left(1+\frac{1+a_{N+1}}{N}\right)^{\beta_{p,N+1}+i_N+1}} \\
&\rightarrow \frac{(1)_{\beta_{p,N+1}}}{\left(1+\frac{1+a_{N+1}}{N}\right)^{\beta_{p,N+1}+1}}.
\end{aligned} \tag{49}$$

Substituting (49) into (48), we obtain (31). The restriction of values of p to the set \mathcal{P}_N , defined in (32), is due to the fact that the high-SNR approximation of the sum over p is dominated by the terms with the largest exponent of SNR (line 2 in (31)), which are the terms with the minimum value of $(\beta_{p,N+1} + \dots + \beta_{p,n})$.

REFERENCES

- [1] Andrea Goldsmith, *Wireless Communications*, Cambridge University Press, 2005.
- [2] Mai Vu and Arogyaswami Paulraj, "MIMO wireless linear precoding", *IEEE Signal Processing Magazine*, vol. 24, no. 5, pp. 86–105, Sep. 2007.

- [3] Emre Telatar, "Capacity of multi-antenna Gaussian channels", *European Transactions on Telecommunications*, vol. 10, no. 6, pp. 585–595, Nov. 1999.
- [4] Petre Stoica and Girish Ganesan, "Maximum-SNR spatial-temporal formatting designs for MIMO channels", *IEEE Transactions on Signal Processing*, vol. 50, no. 12, pp. 3036–3042, Dec. 2002.
- [5] Hemanth Sampath, Petre Stoica, and Arogyaswami Paulraj, "Generalized linear precoder and decoder design for MIMO channels using the weighted MMSE criterion", *IEEE Transactions on Communications*, vol. 49, no. 12, pp. 2198–2206, Dec. 2001.
- [6] Anna Scaglione, Petre Stoica, Sergio Barbarossa, Georgios B Giannakis, and Hemanth Sampath, "Optimal designs for space-time linear precoders and decoders", *IEEE Transactions on Signal Processing*, vol. 50, no. 5, pp. 1051–1064, May 2002.
- [7] Philippe Rostaing, Olivier Berder, Gilles Burel, and Ludovic Collin, "Minimum BER diagonal precoder for MIMO digital transmissions", *Signal Processing*, vol. 82, no. 10, pp. 1477–1480, Oct. 2002.
- [8] D Perez Palomar, John M Cioffi, and Miguel Angel Lagunas, "Joint Tx-Rx beamforming design for multicarrier MIMO channels: A unified framework for convex optimization", *IEEE Transactions on Signal Processing*, vol. 51, no. 9, pp. 2381–2401, Sep. 2003.
- [9] Ludovic Collin, Olivier Berder, Philippe Rostaing, and Gilles Burel, "Optimal minimum distance-based precoder for MIMO spatial multiplexing systems", *IEEE Transactions on Signal Processing*, vol. 52, no. 3, pp. 617–627, Mar. 2004.
- [10] Baptiste Vrigneau, Jonathan Letessier, Philippe Rostaing, Ludovic Collin, and Gilles Burel, "Extension of the MIMO precoder based on the minimum Euclidean distance: A cross-form matrix", *IEEE Journal of Selected Topics in Signal Processing*, vol. 2, no. 2, pp. 135–146, Apr. 2008.
- [11] Saif Khan Mohammed, Emanuele Viterbo, Yi Hong, and Ananthanarayanan Chockalingam, "MIMO precoding with X- and Y-codes", *IEEE Transactions on Information Theory*, vol. 57, no. 6, pp. 3542–3566, Jun. 2011.
- [12] K Pavan Srinath and B Sundar Rajan, "A low ML-decoding complexity, full-diversity, full-rate MIMO precoder", *IEEE Transactions on Signal Processing*, vol. 59, no. 11, pp. 5485–5498, Nov. 2011.
- [13] Linglong Dai, Bichai Wang, Zhiguo Ding, Zhaocheng Wang, Sheng Chen, and Lajos Hanzo, "A survey of non-orthogonal multiple access for 5G", *IEEE communications surveys & tutorials*, vol. 20, no. 3, pp. 2294–2323, 3rd Quart. 2018.
- [14] Qi Wang, Rong Zhang, Lie-Liang Yang, and Lajos Hanzo, "Non-orthogonal multiple access: A unified perspective", *IEEE Wireless Communications*, vol. 25, no. 2, pp. 10–16, Apr. 2018.
- [15] Mojtaba Vaezi, Robert Schober, Zhiguo Ding, and H Vincent Poor, "Non-orthogonal multiple access: Common myths and critical questions", *IEEE Wireless Communications*, vol. 26, no. 5, pp. 174–180, Oct. 2019.
- [16] Yifei Yuan, Zhifeng Yuan, and Li Tian, "5G non-orthogonal multiple access study in 3GPP", *IEEE Communications Magazine*, vol. 58, no. 7, pp. 90–96, Jul. 2020.
- [17] Reza Hoshyar, Ferry P Wathan, and Rahim Tafazolli, "Novel low-density signature for synchronous CDMA systems over AWGN channel", *IEEE Transactions on Signal Processing*, vol. 56, no. 4, pp. 1616–1626, Apr. 2008.
- [18] Reza Hoshyar, Razieh Razavi, and Mohammad Al-Imari, "LDS-OFDM an efficient multiple access technique", in *2010 IEEE 71st Vehicular Technology Conference*. IEEE, May 2010, pp. 1–5.
- [19] Hosein Nikopour and Hadi Baligh, "Sparse code multiple access", in *2013 IEEE 24th Annual International Symposium on Personal, Indoor, and Mobile Radio Communications (PIMRC)*. IEEE, Sep. 2013, pp. 332–336.
- [20] Wissam Abdessamad, Youssef Nasser, Karim Y Kaban, and Oussama Bazzi, "On the performance evaluation of MIMO-SCMA systems", in *2016 8th International Congress on Ultra Modern Telecommunications and Control Systems and Workshops (ICUMT)*. IEEE, Oct. 2016, pp. 135–140.
- [21] Shuai Han, Cheng Guo, Weixiao Meng, Cheng Li, Yang Cui, and Wenyan Tang, "The uplink and downlink design of MIMO-SCMA system", in *2016 International Wireless Communications and Mobile Computing Conference (IWCMC)*. IEEE, Sep. 2016, pp. 56–60.
- [22] Yusha Liu, Lie-Liang Yang, and Lajos Hanzo, "Spatial modulation aided sparse code-division multiple access", *IEEE Transactions on Wireless Communications*, vol. 17, no. 3, pp. 1474–1487, Mar. 2018.
- [23] Zhipeng Pan, Junshan Luo, Jing Lei, Lei Wen, and Chaojing Tang, "Uplink spatial modulation SCMA system", *IEEE Communications Letters*, vol. 23, no. 1, pp. 184–187, Jan. 2019.
- [24] Salma Elkawafi, Abdelhamid Younis, and Raed Mesleh, "Performance analysis of sparse code multiple access MIMO systems", in *2019 IEEE 30th Annual International Symposium on Personal, Indoor and Mobile Radio Communications (PIMRC)*. IEEE, Sep. 2019, pp. 1–6.
- [25] Yusha Liu, Lie-Liang Yang, Pei Xiao, Harald Haas, and Lajos Hanzo, "Spatially modulated multicarrier sparse code-division multiple access", *IEEE Transactions on Wireless Communications*, vol. 19, no. 1, pp. 610–623, Jan. 2020.
- [26] Zhipeng Pan, Wei Liu, Jing Lei, Junshan Luo, Lei Wen, and Chaojing Tang, "Multi-dimensional space-time block coding aided downlink MIMO-SCMA", *IEEE Transactions on vehicular technology*, vol. 68, no. 7, pp. 6657–6669, Jul. 2019.
- [27] Yusha Liu, Luping Xiang, Lie-Liang Yang, and Lajos Hanzo, "Space-time coded generalized spatial modulation for sparse code division multiple access", *IEEE Transactions on Wireless Communications*, Mar. 2021.
- [28] Yang Du, Binhong Dong, Zhi Chen, Pengyu Gao, and Jun Fang, "Joint sparse graph-detector design for downlink MIMO-SCMA systems", *IEEE Wireless Communications Letters*, vol. 6, no. 1, pp. 14–17, Feb. 2017.
- [29] Siyang Tang, Li Hao, and Zheng Ma, "Low complexity joint MPA detection for downlink MIMO-SCMA", in *2016 IEEE Global Communications Conference (GLOBECOM)*. IEEE, Dec. 2016, pp. 1–4.
- [30] Sanjeev Sharma, Kuntal Deka, and Baltasar Beferull-Lozano, "Low-complexity detection for uplink massive MIMO SCMA systems", *IET Communications*, vol. 15, no. 1, pp. 51–59, Jan. 2021.
- [31] Zhipeng Pan, Jing Lei, Lei Wen, Chaojing Tang, and Zhongfeng Wang, "Low-complexity sphere decoding for MIMO-SCMA systems", *IET Communications*, vol. 15, no. 4, pp. 537–545, Mar. 2021.
- [32] Marco Chiani, Moe Z Win, and Alberto Zanella, "On the capacity of spatially correlated MIMO Rayleigh-fading channels", *IEEE Transactions on Information Theory*, vol. 49, no. 10, pp. 2363–2371, Oct. 2003.
- [33] Marco Chiani, Davide Dardari, and Marvin K Simon, "New exponential bounds and approximations for the computation of error probability in fading channels", *IEEE Transactions on Wireless Communications*, vol. 2, no. 4, pp. 840–845, Jul. 2003.
- [34] Milton Abramowitz and Irene A Stegun, *Handbook of Mathematical Functions with Formulas, Graphs, and Mathematical Tables. National Bureau of Standards Applied Mathematics Series 55. Tenth Printing.*, ERIC, 1972.
- [35] John G Proakis and M Salehi, *Digital Communications*, McGraw-Hill Inc., New York, 1995.
- [36] Zhengdao Wang and Georgios B Giannakis, "A simple and general parameterization quantifying performance in fading channels", *IEEE Transactions on Communications*, vol. 51, no. 8, pp. 1389–1398, Aug. 2003.
- [37] Joseph Boutros, Emanuele Viterbo, Catherine Rastello, and J-C Belfiore, "Good lattice constellations for both Rayleigh fading and Gaussian channels", *IEEE Transactions on Information Theory*, vol. 42, no. 2, pp. 502–518, Mar. 1996.
- [38] Monirosharieh Vameghestabhanati, Ian D Marsland, Ramy H Gohary, and Halim Yanikomeroglu, "Multidimensional constellations for uplink SCMA systems—A comparative study", *IEEE Communications Surveys & Tutorials*, vol. 21, no. 3, pp. 2169–2194, Apr. 2019.
- [39] Mahmoud Taherzadeh, Hosein Nikopour, Alireza Bayesteh, and Hadi Baligh, "SCMA codebook design", in *2014 IEEE 80th Vehicular Technology Conference (VTC2014-Fall)*. IEEE, Sep. 2014, pp. 1–5.
- [40] Jaap Van De Beek and Branislav M Popovic, "Multiple access with low-density signatures", in *GLOBECOM 2009-2009 IEEE Global Telecommunications Conference*. IEEE, Dec. 2009, pp. 1–6.
- [41] European Telecommunications Standards Institute, "5G; NR; Multiplexing and channel coding", *European Telecommunications Standards Institute*, 3GPP TS 38.212 version 15.2.0 Release 15, Jul. 2018. [Online] Available: https://www.etsi.org/deliver/etsi_ts/138200_138299/138212/15.02.00_60. [Accessed: Sep. 28, 2021].